IJCRT.ORG ISSN : 2320-2882

INTERNATIONAL JOURNAL OF CREATIVE RESEARCH THOUGHTS (IJCRT)

An International Open Access, Peer-reviewed, Refereed Journal

Investigating The Thermal Characteristics Of A Composite Phase-Change Material Made Of Nano-Tubular Tio_2 And Paraffin For Use In Thermal Energy Storage Applications

[1] Anitha Manisekaran, [2] Ramalingam A, [3] Meera C

[1]Research Scholar, [2]Associate Professor, [3]Associate Professor

[1]Department of Physics, Barathiyar University, Coimbatore, India.

[2]Department of Physics, Government Art college, Udumalpet, India.

[3]Department of Master of Business Administration, Dr.N.G.P. Institute of Technology, Coimbatore, India.

Abstract: In energy management systems, phase change materials (PCM) thermal energy storage (TES) is crucial. Due to its distinct thermal and physical characteristics, paraffin offers a wide range of uses as a PCM. This study is the first to synthesise nano titanium oxide in a tubular shape and in powder form. This paper investigates the properties of nanoparticle-enhanced phase change material (PCM) on solar still process and performance. Solar energy is a renewable energy source that can be utilized for different applications in day-to-day life. An effective method of storing thermal energy from solar is through the use of phase change materials PCMs with titanate. The future demand will be high and fresh water resources are getting depleted at a faster rate. Solar still is a very simple device for converting the available brackish water into potable water. The main drawback of passive type solar still is its lower efficiency and distillate output. The usage of NPCM enhances the still productivity especially after the sunset. The anatase sample obtained less intensive peak than rutile peak at approximate wavelength of 300 nm shown in UV spectrum. The bands around 734 cm-1 correspond to intrinsic stretching vibration of metal ion at the tetrahedral site. The formations of spindle like structure are shown in TEM image, sample gives the average diameter is 33 nm of TiO2 nanoparticles. The strong excitation peak centered at 298.96 nm indicates a violet emission band is occurred. Solar still with titanium oxide nanoparticles enhanced the yielded up to 4910 ml/m2/day. These results will benefit to the researcher can further investigate on solar power generation, water heating system, solar cookers, and solar still using NPCMs for commercial development.

Index Terms **-** Phase change materials, Thermal energy storage, Paraffin, Nano-tubular zinc oxide.

I. INTRODUCTION

In the fields of electronics, optics, solar cells, field effect transistors, photo detectors, and gas sensors, zinc oxide is a material that shows promise [1]. It is a promising material for numerous applications in these sectors due to its broad bandgap (3.4 eV) semiconductor and high exciton binding energy (60 MeV) [2-3]. Zinc oxide optical, electrical, and conductivity properties are altered by the incorporation of transition metal impurities. Zinc oxide has had its characteristics changed by the incorporation of several metals, including Mn, Fe, Co, Ni, etc [4]. Metal doped zinc oxide has been created using a number of techniques, including chemical vapour deposition (CVD) technique [5]. Sol-gel method, [6] arc discharge [7], and laser ablation [8]. Due of the simple reaction conditions, higher yield, and desirable forms of nanomaterials, the sol-gel process is used. These techniques produce nanoparticles that can be used to create nanocomposites. Nanocomposites are a new class of materials made with nanosized fillers. Organic-inorganic hybrids are nanoscale inorganic particles doped in organic polymers [9]. Due to the significant interfacial interaction between the organic moieties and inorganic nanoparticles, Zn1-xCoxO is integrated into polymers to improve their mechanical and optical properties [10]. The water-soluble and easily biodegradable in nature, polyvinyl alcohol (PVA) serves as an environmentally friendly polymer [11]. Metal oxide can be used to create thin films with ease. PVA polymer exhibits strong absorption characteristics in the ultraviolet (UV) spectrum between 300 and 500 nm [12].

In the current paper, we describe the synthesis of various cobalt-doped zinc oxide concentrations utilised to create PVA nanocomposite films [13]. Spectroscopic methods such as UV-Vis absorption spectroscopy and photoluminescence (PL) were used to characterise the films. Thermogravimetric analysis (TGA), powder X-ray diffraction (XRD), scanning electron microscopy (SEM), atomic force microscopy (AFM), and energy-dispersive X-ray spectroscopy (EDX) were used to examine the thermal and morphological features. By using Fourier transform infrared spectroscopy (FTIR), the functional group was studied.

The purpose of this work was to develop tubular nano ZnO powder as an additive to enhance the thermal properties of paraffin as PCM for TES applications. This will open up a new market for ZnO products in addition to its many benefits. evaluating the chemical and thermal properties of the composite of ZnO and paraffin (ZnO-P) with those of pure paraffin.

2. EXPERIMENTAL DETAILS

2.1. Materials

The production of Co-doped titanium oxide nanowires was carried out using the technique described by Yuhas et al [14]. In a round-bottomed flask with 25 ml of trioctyl amine, zinc acetate (0.5838 g, 2.66 mol%) and cobalt (II) acetate (0.0324 g, 0.05 equiv., 0.13 mol%) were combined. The condenser-equipped flask was quickly heated to 300°C. The solution's colour shifted from colourless to royal blue as the solid disintegrated. The solution's colour changed to green after 20-25 minutes, signalling the start of the nanowire production process. After 180 minutes of reaction time, the liquid was cooled to room temperature and repeatedly washed with ethyl alcohol to eliminate any cobalt impurities. According to what was written in the literature, the green suspensions were kept in ethanol [15]. This answer remained reliable for several months. The mean nanowire yield during synthesis was 45 mg [16-20].

The following stage involved dispersing various concentrations of Zn0.95Co0.05O (0.8, 1.2, 1.5, and 2.0 mol%) in methanol using a sonicator for 30 minutes to create solution A. Solution B was created by dispersing 0.4 g of PVA in 20 ml of deionized water for roughly 30 minutes. Drop by drop, while stirring, solution A was mixed with solution B until the latter's colour changed to a light green and became translucent. The resulting mixture was put onto a Petri plate, sonicated for about 30 minutes, and then heated to 60°C for 48 hours [21-24]. This technique was used to create thin composite films with various compositions.

2.2. Still Set up

The real area of the water storage basin still is 1 square metre, and its dimensions are 100 cm by 100 cm by 8 cm illustrated in Fig.1. The still is constructed from a sheet of aluminium with a 1 mm thickness that has been painted black to better absorb solar radiation. Two 4 mm thick glass plates are positioned at the top of the basin and are inclined at an angle of 12o to the horizontal, which is similar to the location's latitude. During the day, solar radiation generally falls on the glass plates surface. The metal box, which measures 113 cm x 113 cm x 20 cm, contains the basin. Sawdust was used as insulation in the space between the basin and the exterior metal box. Insulation belt thickness is 10 cm at the bottom and 5 cm on either side. On both sides of the still, a channel is created beneath the lower margins of the glass to collect condensed water.

The water is continuously drained down the pipe and kept in a measuring jar after collection. Thermal wires can be inserted through a hole in the side wall of the basin to measure the water, basin, and PCM tube temperatures. To prevent heat and vapour loss, insulation material was applied at the hole.

Fig. 1. Schematic view of single basin double slope solar still

In the months of April and May 2023, the experiment was run. K-type thermocouple wires that have been calibrated in conjunction with a digital multimeter were used to measure the temperatures of the water, basin, PCM tube, and glass top cover. An alcohol thermometer is used to measure the ambient temperature, and an electronic anemometer is used to detect the wind speed. The solar radiation was measured with a pyranometer, and the hourly distillate yield was recorded in a measuring jar. During the trial days, all the environmental and operational data were measured and recorded for each hour from 10 am to 10 pm.

2.3. TiO_2 Nanoparticle Preparation

Titanium nitrate Ti(NO3)2, the basic materials for the synthesis of TiO2 nanoparticles were 6H2O and deionized water. Ti(NO3)2 solution, 0.2 ml. In order to make 6H2O, 150 ml of deionized water was used. The solution was then heated to 400o C and calcined. The first phase of the procedure uses a [Ti(NO3)2]0.2 solution. Using 150 ml of deionized water, 6H2O was created. This step was adhered to by prior researchers creating their metal oxide nanoparticle production process. The precursor solution of ammonia was gradually and drop by drop introduced to the [Ti(NO3)2] during the second step of the procedure. 6H2O mixture. The solutions PH level is kept between 8 and 10.

This solution-adding process takes three hours. In the third step, the solution mixture was continuously swirled for five hours. This procedure was continued up until the dark silver colour of the precursor changed. As the fourth step of the procedure, the settled precipitation was filtered and dried at 100° C to remove the water vapour. As the last step of the synthesis process, the sample was calcined once more for three hours at 400 degrees Celsius. Precipitations influence on the reaction was full. These components were also taken out of the by product. So, the undesired contaminants were removed with the help of the calcination's procedure at 400^{o}C.

2.4. Preparation of NPCM

An electric heater was used to heat the paraffin wax to 10oC over its melting point, and SDBS was then added to PCM at a 1:1 ratio to the nanoparticles. The surfactants job was to make sure that the TiO2 nanoparticles in paraffin wax were distributed uniformly Fig.2. TiO2 nanoparticles (0.1 weight percent) were then added. Based on a survey of the literature, the mass fraction of 0.1% was decided. To keep the PCM in a liquid state throughout the whole procedure, the temperature of the vibrator was kept at 10oC shown in Fig.2.

Fig.2. Schematic for Preparation of NPCM

2.5. Mechanism

The PCM tubes and the basin water are heated by the sunshine that enters through the glass cover. The basin liner absorbs the heat energy, and some of it is transferred to the basin water through convection and some to the PCM tubes through conduction. The PCM inside the tubes is heating up and melting as it does so. The PCM starts to melt at this point. The heat will be kept as a sensible heat in the fully melted PCM once it has melted. After noon, the sun radiation starts to decline, and the still components begin to cool. During periods of low solar radiation and at night, the PCM will serve as a source of heat for the water in the basin. Due to coppers excellent thermal conductivity, heat is quickly transferred to the basin water, keeping it still during the three still operation modes with and without PCM. Throughout the experiment, it was noted that the PCM tubes in the still caused the water in the basin to become warmer. At 2 pm, the water temperature in a still with a PCM reaches its highest point before beginning to fall. At this point, the liquid PCM begins to energise the still water.

3. Results and discussion

3.1. Powder X-Ray diffraction Method

In general, low intensity and rather large diffraction peaks can be seen in the powder X-ray diffraction patterns. The powder X-ray diffraction patterns of titanium oxide nanoparticles are shown in Fig.3. According to powder X-ray diffraction patterns, the primary peaks of titanium dioxide nanoparticles rutile phase include 27.506 (110), 36.040 (101), 41.185 (111), 44.140 (210), 54.231 (211), 56.781 (220), 62.258 (002), and 68.996 (301). The ICDD number 00-001-1292, which corresponds to rutile, can be used to index all of the lines in this pattern [12]. The pattern lacked any more steps. The Debye-Scherrer equation was used to calculate the crystallite size for the prepared samples by measuring the broadening of the phase main peaks most intense peak in a diffraction pattern linked to a specific planar reflection inside the crystal unit cell.

$$D = \frac{k\lambda}{\beta \cos\theta}$$

The wavelength of the X-ray radiation that is extracted from the Cu-K source is, the diffraction angle is, and the full width at half maximum is, where k is the shape factor, which has a constant value of 0.94. According to Scherer's formula, crystallite sizes typically range between 40 and 50 nm.

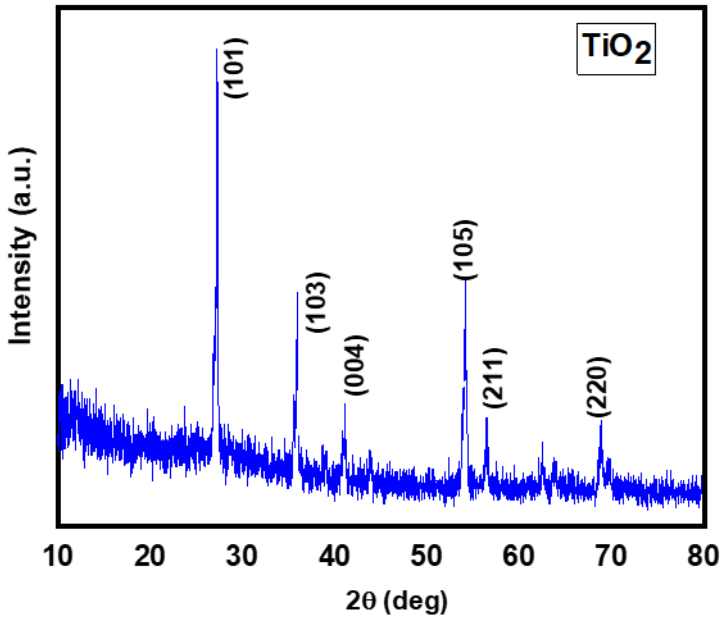

Fig.3. Powder X-ray diffraction pattern of TiO_2 nanoparticles

3.2. U-V Visible Spectroscopy

The prepared samples TiO2 nano pigments UV-visible absorption spectra are shown in Fig.4. As can be seen from the spectra, the rutile sample exhibits the narrowest, most intense peak at 320 nm, which is in line with its well-known high refractive index and high brightness. According to powder X-ray diffraction examination, the peak produced in the anatase and brookite samples is wider than the other peak because the two phases are present in the samples. At a wavelength of about 300 nm, the anatase sample produced a peak that was less intense than the rutile peak.

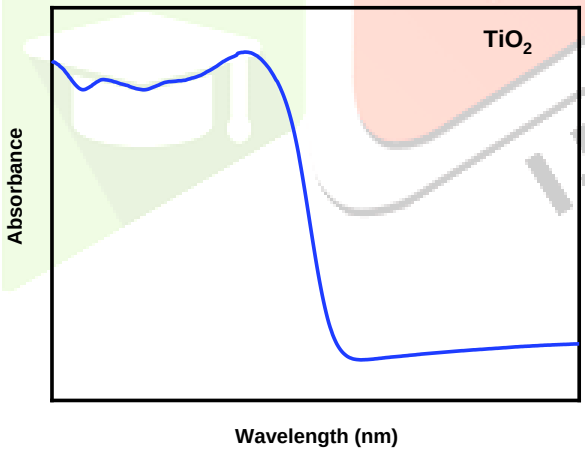

Fig.4. UV-Visible Spectroscopy of TiO_2 nanoparticles

3.3. FTIR spectrum

In the FTIR spectrum, bands of titanium dioxide nanoparticles are seen in Fig.5. The bands at 734 cm^{-1} are a result of the metal ions tetrahedral sites intrinsic stretching vibration. The stretching vibration of the OH group is assigned a peak at about 1653 cm^{-1}, and the Ti-O vibration likewise reached a peak at 734 cm^{-1}.

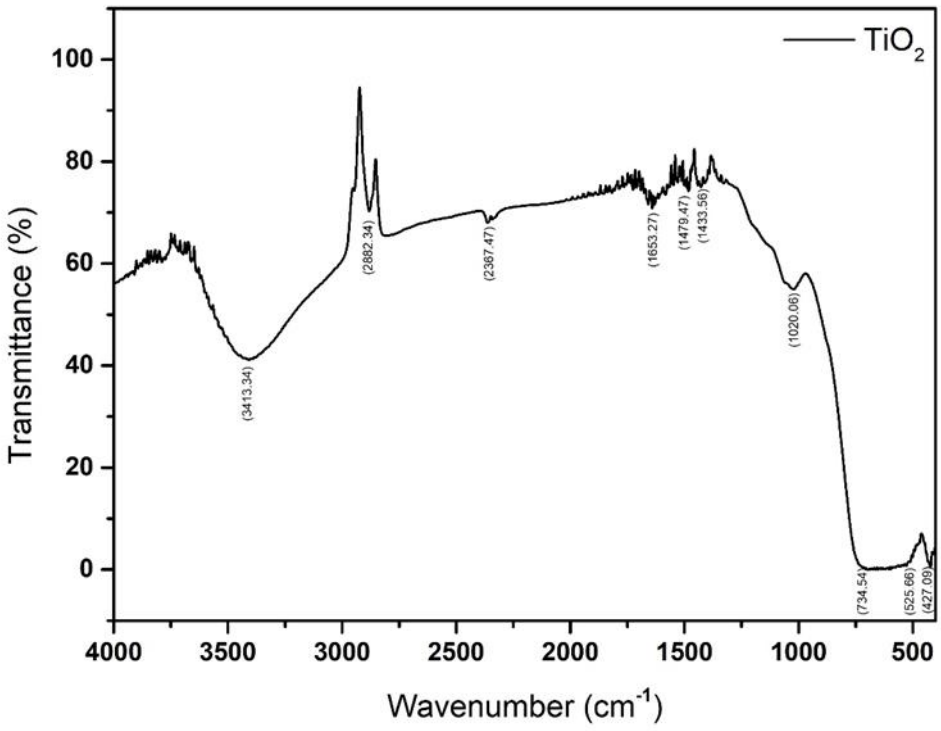

Fig.5. FTIR Spectroscopy of TiO_2 nanoparticles

3.4 TEM Analysis

TiO_2 nanoparticles are shown in a transmission electron microscope image in Fig.6. The TEM image shows a detailed magnification of the sample that was previously processed.

The modest agglomeration of the nanoparticle morphologies demonstrates that the spherical nanoparticles are adhered to the thin platelets, as depicted in the figure.

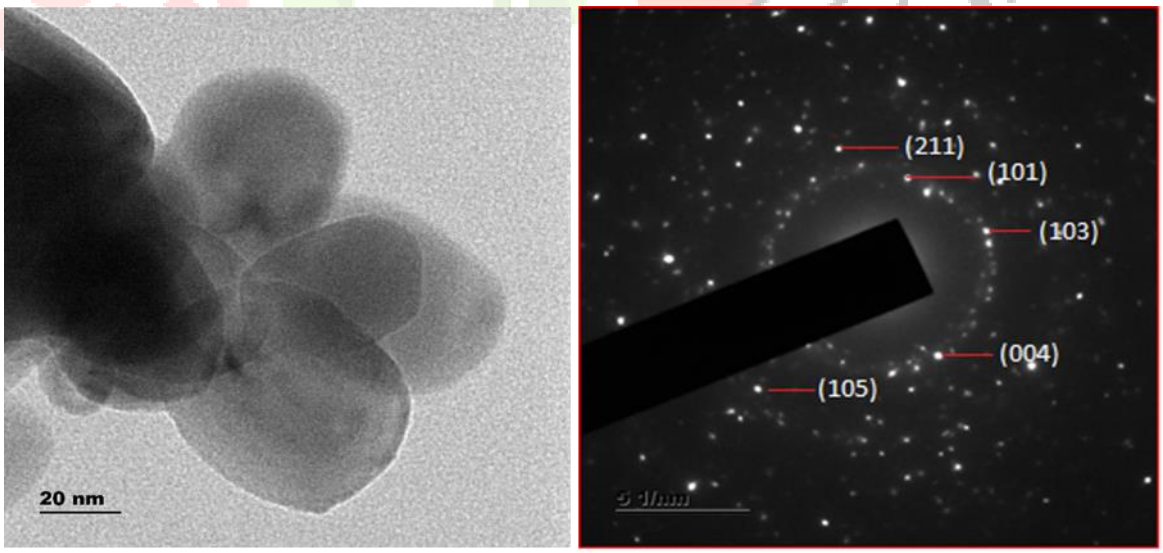

Fig.6. TEM images of TiO_2 nanoparticles

When compared to other shapes, elongated spherical shaped particles have a large surface area. It develops as a result of the usage of ammonia in the synthesis process. Fig.5. depicts the development of spindle-like structures. The samples TEM picture reveals TiO2 nanoparticles with an average diameter of 33 nm. The TiO2 nanoparticles are crystalline according to the selected area electron diffraction (SAED) patterns. The concentric circles of the SAED pattern are nicely matched with the diffraction planes of the corresponding major peaks as seen in the powder X-ray diffraction.

3.5 Photo Luminescence Analysis

The TiO_2 nanoparticles photoluminescence spectra were seen at room temperature, as depicted in Fig.7. There is a violet emission band for the material, according to the strong excitation peak with a centre wavelength of 298.96 nm. TiO2 nanoparticles assigned peak intensity of the curve is 11.52 (a.u). When the molecule is present at 320 nm, TiO2 nanoparticles emit violet light at a wavelength of 298.96 nm. According to the observation, titanium oxide may cause a molecule to undergo an intersystem crossover, which results in fluorescence.

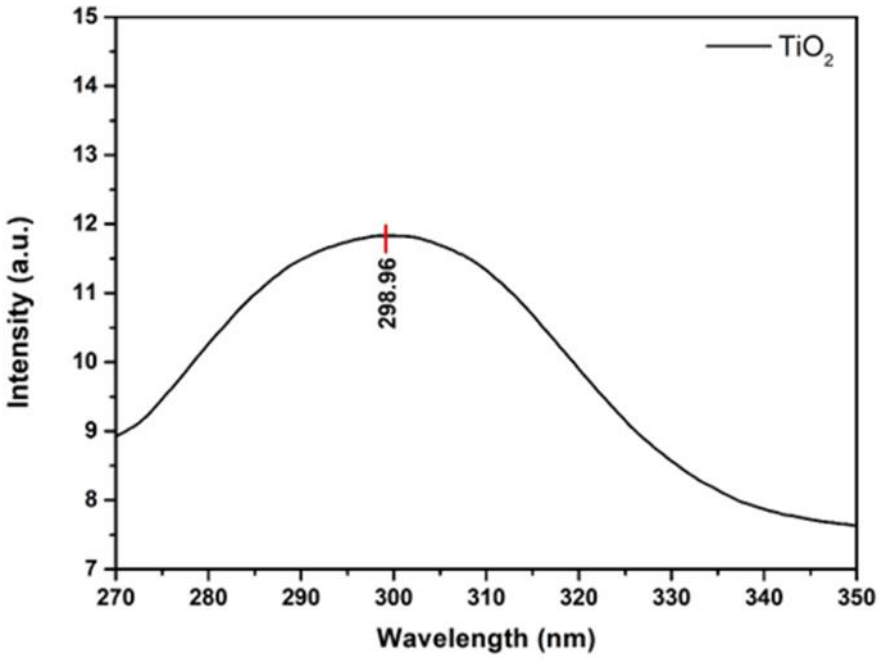

Fig.7. Photo Luminescence of TiO_2 nanoparticles

Single band emission at 298.96 nm for the samples is indicative of good TiO2 nanoparticle crystallinity.

3.6 Solar radiation and ambient temperature

The productivity rate of solar stills is mostly hampered by solar radiation. The difference between the ambient temperature and solar insolation with respect to time is shown in Fig.8. The ambient temperature was recorded to be between 31°C and 38°C, while the sun radiation was measured to reach a maximum of 1426 W/m2.

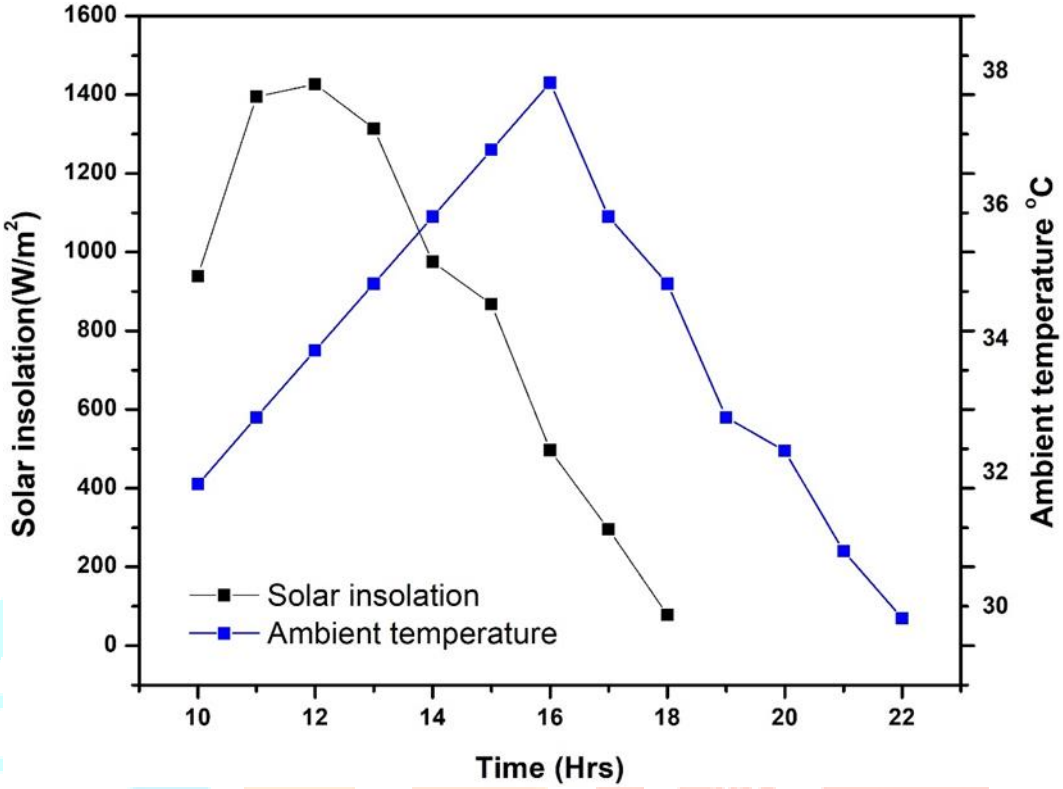

Fig.8. Hourly variation of solar insolation and ambient temperature with respect to time

The productivity rate of solar stills is mostly hampered by solar radiation. The difference between the ambient temperature and solar insolation with respect to time is shown in Fig.8. The ambient temperature was recorded to be between 31°C and 38°C, while the sun radiation was measured to reach a maximum of 1426 W/m2.

3.6.1 Hourly variation of temperature of solar still with PCM tube and NPCM tube

Fig.9. shows the hourly variation of the temperature of the glass top, water, basin, PCM tube, and NPCM tube with respect to time. The PCM tube temperature was found to be slightly higher until 3 or 4 pm. Following that, the system components begin to cool as the sun sets, and at around 5 or 6 O'clock in the evening, PCM and NPCM activity begins.

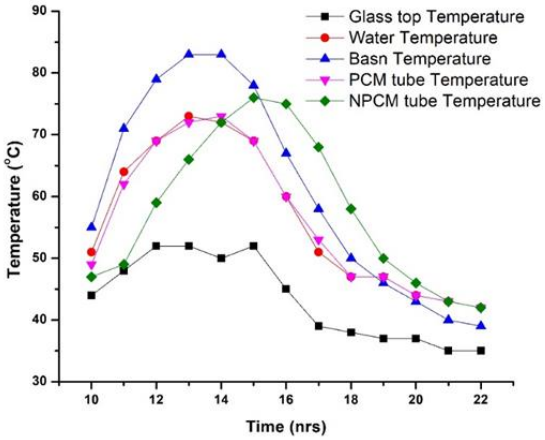

Fig.9. Hourly variation of temperature of solar still with PCM and NPCM

It should be obvious that the water temperature is now higher than that of the PCM and NPCM tubes. This is as a result of the liquid PCM beginning to crystallise and transferring its heat to the basin water and cooling. This approach is used until the PCM and water are in thermal equilibrium. The hourly change of the water's temperature, the temperature of the basin, the temperature of the PCM and NPCM tubes, and the temperature of the solar still's exterior glass cover with respect to time. The greatest basin temperature recorded was 84oC, while the extreme aquatic temperatures for PCM and NPCM were 73oC and 76oC, respectively. The glass temperature was also found to be between 40 and 52 degrees Celsius. The highest temperature reached for PCM tubes was 73°C, whereas the highest temperature for NPCM tubes was 76°C.

3.6.2 Hourly variation of glass temperature of solar still without, with PCM and NPCM

The hourly variations in glass temperature for the stills with PCM, PCM and NPCM are shown in Fig.10. For the three ways of the still, the glass temperature reaches its peak at 2 pm when the solar insolation is at its highest. It is evident that after 5 O'clock, stills without and with PCM have slightly better glass temperatures.

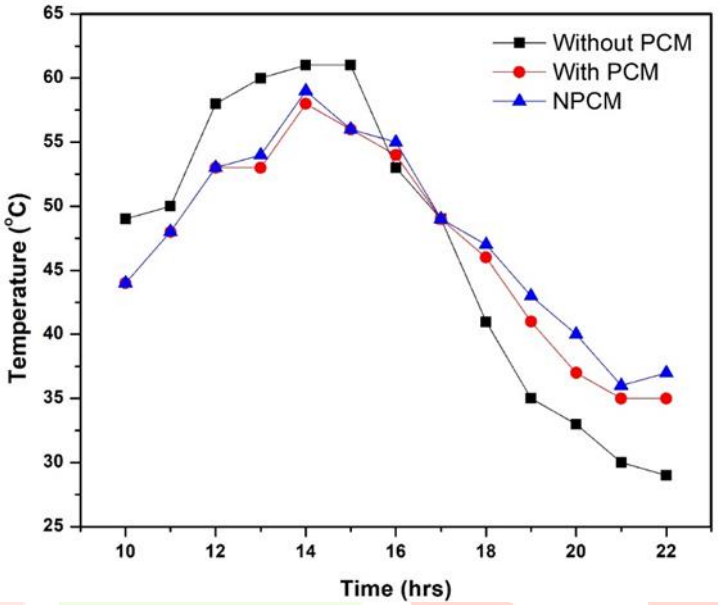

Fig.10. Hourly variation of glass temperature of solar still with, without PCM and NPCM

3.6.3 Hourly variation of basin temperature of solar still without, with PCM and NPCM

The relative analysis of the hourly still efficiency for the three still modes without PCM, with PCM, and with NPCM is shown in Fig.11. At 2 pm, when solar insolation was at its highest, the three modes of still produced the most sublime essence. The extract yield from the still without PCM was around 3680 ml/m2/day, the distillate output from the still with PCM tubes was about 4690 ml/m2/day, and the concentrate output from the still with NPCM tubes was about 4910 ml/m2/day.

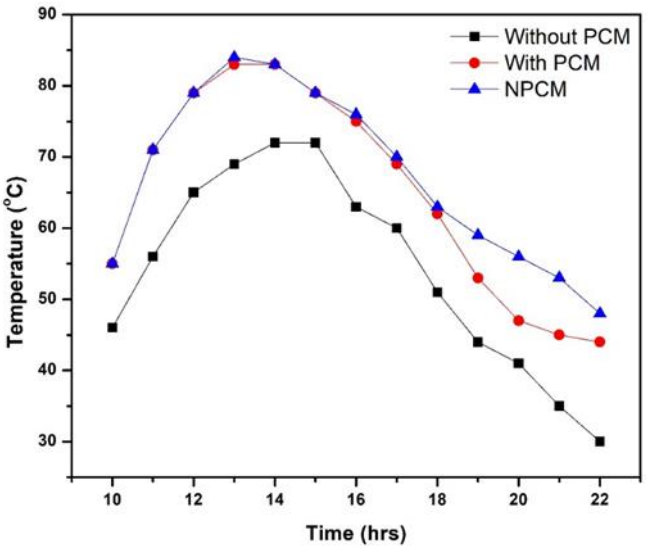

Fig.11. Hourly variation of basin temperature of solar still with, without PCM and NPCM

3.6.4 Hourly variation of water temperature of solar still with NPCM

Fig.12. clearly shows the relationship between the rate of reduction in aquatic temperature and time. Even after dusk, this device prolongs the vanishing process. Conventional solar stills produced distillate up until 8 p.m., while stills with PCM produced distillate until 12 a.m. Thus, it was shown that using NPCM tubes increases the desalination systems distillation time by up to 6 to 7 hours after sunset. The ambient temperature was recorded in the range of 45°C to 80°C, while the solar radiation was measured in the range of 296 W/m2 to 1426 W/m2.

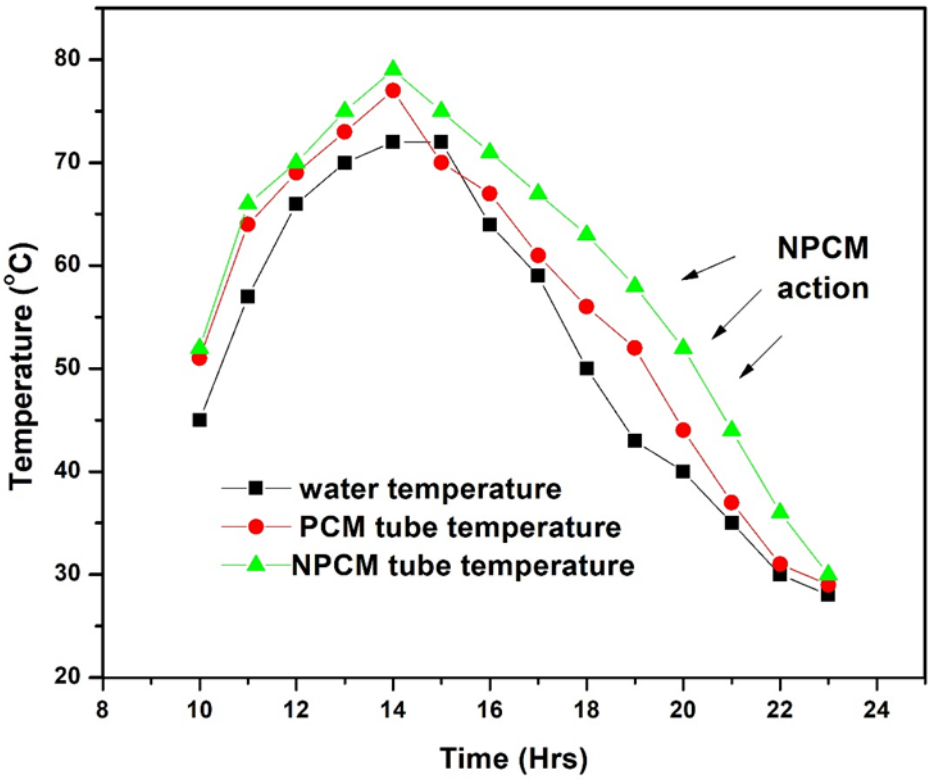

Fig. 12. Hourly variation of water temperature of solar still with PCM and NPCM

Demonstrates the hourly variation of water, PCM tube and NPCM tube temperature with respect to time. It was observed that the NPCM tube temperature is moderately greater till 3 pm. After that when the solar radiation starts to fall the system components are getting cooler and the NPCM action starts to take place at 5 pm. It is clearly noticed that the water and PCM tube temperature becomes lesser than NPCM tubes temperature.

This is due to that the liquid NPCM starts to solidify and transfer its heat to the basin water and receiving cooler. This process remains till the NPCM and water reach thermal symmetry with each other. The comparative analysis of hourly still productivity for the two modes of the still, with and without NPCM. The supreme distillate output was obtained at 2pm for the two modes of the still when the solar sunstroke was high. The still with PCM produced distillate production about 4690 ml/m2/day whereas the still with NPCM tubes produced the distillate output about 4910ml/m2/day.

4. Conclusion

Due to its availability and capacity to improve system performance, energy storage is particularly alluring to a wide range of parties. Knowledge expansion is more viable and effective than the construction of new power plants when extra energy is stored for later use. Due to the latent heat of the phase change materials, PCMs and NPCMs can be extremely useful in storing larger amounts of thermal energy. The fixed temperature of the phase change materials in NPCMs also supports a target-oriented settling temperature. Numerous factors still have an impact on the thermal energy storage capability of NPCMs in solar heat recovery. The judgements below were made in light of the findings.

1. When compared to other shapes, the surface area of extended spherical shaped atoms in TiO2 nanoparticles is high.

2. A solar still that used titanium oxide nanoparticles in addition to phase change materials demonstrated a 22% increase in efficiency over a solar still that used only phase change materials.

3. The distillate productivity from the still without PCM was around 3680 ml/m2/day, while the distillate output from the still with PCM tubes was about 4690 ml/m2/day and the distillate output from the still with titanium oxide nanoparticles improved phase change materials tubes was about 4910 ml/m2/day.

4. As opposed to the usage of PCM in solar still applications, saturation of titanium oxide nanoparticles in phase change materials has well potential.For this study secondary data has been collected. From the website of KSE the monthly stock prices for the sample firms are obtained from Jan 2010 to Dec 2014. And from the website of SBP the data for the macroeconomic variables are collected for the period of five years. The time series monthly data is collected on stock prices for sample firmsand relative macroeconomic variables for the period of 5 years. The data collection period is ranging from January 2010 to Dec 2014. Monthly prices of KSE -100 Index is taken from yahoo finance.

REFERENCES

1. Xi, Peng, Yuqing Duan, Pengfei Fei, Lei Xia, Ran Liu, and Bowen Cheng. "Synthesis and thermal energy storage properties of the polyurethane solid–solid phase change materials with a novel tetrahydroxy compound." European polymer journal 48, no. 7 (2012): 1295-1303.

2. Athikesavan, Venkatraj, M. Arulmani, and S. Bhuvana. "Evaluation of the structure and electrical properties of (1-x) Bi0.5(Na0.80K0.20)0.5TiO3–xLiNbO3 ceramic composite for piezoelectric sensor applications." International Journal of Modern Physics B (2023): 2350280.

3. Fernandes, D., F. Pitié, G. Cáceres, and J. Baeyens. "Thermal energy storage:“How previous findings determine current research priorities”." Energy 39, no. 1 (2012): 246-257. https://doi.org/10.1016/j.energy.2012.01.024.

4. Chen, Changzhong, Wenmin Liu, Hongwei Wang, and Lanlan Zhu. "Synthesis and characterization of novel solid-solid phase change materials with a polyurethaneurea copolymer structure for thermal energy storage." RSC advances 6, no. 105 (2016): 102997-103005. DOI: 10.1039/C6RA23141A.

5. R. N. Perumal, V. Athikesavan, P. Nair. Influence of lead titanate additive on the structural and electrical properties of Na0.5Bi0.5TiO3-SrTiO3 piezoelectric ceramics. Ceram. Int. 44 (2018) 13259-13266.

6. R. N. Perumal, V. Athikesavan. Investigations on electrical and energy storage behaviour of PZN-PT, PMN-PT, PZN–PMN-PT piezoelectric solid solutions. J. Mater Sci: Mater Electron (2019) 30: 902.

7. Arunkumar, T., Ramalingam Velraj, David C. Denkenberger, Ravishankar Sathyamurthy, K. Vinoth Kumar, and Amimul Ahsan. "Productivity enhancements of compound parabolic concentrator tubular solar stills." Renewable energy 88 (2016): 391-400. https://doi.org/10.1016/j.renene.2015.11.051.

8. Abujazar, Mohammed Shadi S., Suja Fatihah, Ibrahim Anwar Ibrahim, A. E. Kabeel, and Suraya Sharil. "Productivity modelling of a developed inclined stepped solar still system based on actual performance and using a cascaded forward neural network model." Journal of Cleaner production 170 (2018): 147-159. https://doi.org/10.1016/j.jclepro.2017.09.092.

9. Ramazanov, M. A., F. V. Hajiyeva, A. M. Maharramov, A. B. Ahmadova, U. A. Hasanova, A. M. Rahimli, and H. A. Shirinova. "Influence of polarization processes on the morphology and photoluminescence properties of PP/TiO2 polymer nanocomposites." Acta Phys. Pol. A 131, no. 6 (2017): 1540. DOI: 10.12693/APhysPolA.131.1540.

10. Perumal, Rajesh Narayana, and Venkatraj Athikesavan. "Structural and electrical properties of lanthanide-doped Bi0.5(Na0.80K0.20)0.5TiO3-SrZrO3 piezoelectric ceramics for energy-storage applications." Journal of Materials Science: Materials in Electronics 31 (2020): 4092-4105

11. Nazir, Hassan, Mariah Batool, Francisco J. Bolivar Osorio, Marllory Isaza-Ruiz, Xinhai Xu, K. Vignarooban, Patrick Phelan, and Arunachala M. Kannan. "Recent developments in phase change materials for energy storage applications: A review." International Journal of Heat and Mass Transfer 129 (2019): 491-523. https://doi.org/10.1016/j.ijheatmasstransfer.2018.09.126.

12. Athikesavan, Venkatraj, E. Ranjith Kumar, and J. Suryakanth. "Evaluation of the structural and electrical properties of perovskite NKN-LN ceramics for energy storage applications." New Journal of Chemistry 46.42 (2022): 20433-20444.

13. Singh, Randeep, Sadegh Sadeghi, and Bahman Shabani. "Thermal conductivity enhancement of phase change materials for low-temperature thermal energy storage applications." Energies 12, no. 1 (2019): 75. https://doi.org/10.3390/en12010075.

14. Boy, E., R. Boss, and M. Lutz. "A collector storage module with integrated phase change material." In Proc. ISES, pp. 3672-3680. Pergamon Press, Hamburg, 1987.

15. Hepbasli, Arif, and Zeyad Alsuhaibani. "A key review on present status and future directions of solar energy studies and applications in Saudi Arabia." Renewable and sustainable energy reviews 15, no. 9 (2011): 5021-5050. https://doi.org/10.1016/j.rser.2011.07.052.

16. Kuta, Marta, Dominika Matuszewska, and Tadeusz Michał Wójcik. "The role of phase change materials for the sustainable energy." In E3S Web of conferences, vol. 10, p. 00068. EDP Sciences, 2016. https://doi.org/10.1051/e3sconf/20161000068.

17. Wei, Z., Z. Heping, and Y. Yongke. "Dielectric and piezoelectric properties of Y2O3 doped (Bi0.5Na0.5) 0.94Ba0.06TiO3 lead-free piezoelectric ceramics." Key Engineering Materials 105 (2007): 336-338.

18. Mofijur, Mahlia, Teuku Meurah Indra Mahlia, Arridina Susan Silitonga, Hwai Chyuan Ong, Mahyar Silakhori, Muhammad Heikal Hasan, Nandy Putra, and S. M. Rahman. "Phase change materials (PCM) for solar energy usages and storage: an overview." Energies 12, no. 16 (2019): 3167. https://doi.org/10.3390/en12163167.

19. Athikesavan, Venkatraj, S. Bhuvana, and G. Thilakavathi. "Structural and Electrical Properties of Pb(Mg1/3Nb2/3)O3-Pb(Yb1/2Nb1/2)O3-PbTiO3 Ternary Ceramic for Energy Storage Application." Ferroelectrics letters section 49.4-6 (2022): 104-110

20. Zhang, Zhe, Zhen Zhang, Tian Chang, Juan Wang, Xin Wang, and Guofu Zhou. "Phase change material microcapsules with melamine resin shell via cellulose nanocrystal stabilized Pickering emulsion in-situ polymerization." Chemical Engineering Journal 428 (2022): 131164. https://doi.org/10.1016/j.cej.2021.131164.

21. Gorbacheva, Svetlana N., Veronika V. Makarova, and Sergey O. Ilyin. "Hydrophobic nanosilica-stabilized graphite particles for improving thermal conductivity of paraffin wax-based phase-change materials." Journal of Energy Storage 36 (2021): 102417. https://doi.org/10.1016/j.est.2021.102417.

22. Maher, Hisham, Kaiser Ahmed Rocky, Ramadan Bassiouny, and Bidyut Baran Saha. "Synthesis and thermal characterization of paraffin-based nanocomposites for thermal energy storage applications." Thermal Science and Engineering Progress 22 (2021): 100797. https://doi.org/10.1016/j.tsep.2020.100797.

23. Avargani, Vahid Madadi, Brian Norton, Amir Rahimi, and Hajir Karimi. "Integrating paraffin phase change material in the storage tank of a solar water heater to maintain a consistent hot water output temperature." Sustainable Energy Technologies and Assessments 47 (2021): 101350. https://doi.org/10.1016/j.seta.2021.101350.

24. Abdeali, Golnoosh, Mahdi Abdollahi, and Ahmad Reza Bahramian. "Synthesis and characterization of paraffin wax nanocapsules with polyurethane shell (PU/PW); the droplet size distribution: A key factor for thermal performance." Renewable Energy 163 (2021): 720-731. https://doi.org/10.1016/j.renene.2020.09.013.